Organic & Biomolecular Chemistry

COMMUNICATION

View Article Online
View Journal | View Issue

Cite this: *Org. Biomol. Chem.*, 2019, **17**, 7863

Received 17th May 2019,
Accepted 2nd July 2019

DOI: 10.1039/c9ob01161g

rsc.li/obc

Distortion of mannoimidazole supports a $B_{2,5}$ boat transition state for the family GH125 α-1,6-mannosidase from *Clostridium perfringens*

Alexandra Males,[a] Gaetano Speciale,[b] Spencer J. Williams *[b] and Gideon J. Davies *[a]

Enzyme transition-state mimics can act as powerful inhibitors and allow structural studies that report on the conformation of the transition-state. Here, mannoimidazole, a mimic of the transition state of mannosidase catalyzed hydrolysis of mannosides, is shown to bind in a $B_{2,5}$ conformation on the *Clostridium perfringens* GH125 α-1,6-mannosidase, providing additional evidence of a $^{O}S_2$–$B_{2,5}$–$^{1}S_5$ conformational itinerary for enzymes of this family.

A conformational itinerary describes how a molecule changes shape along a reaction coordinate. For reactions catalysed by enzymes, the three-dimensional fold of the protein and its electrostatic microenvironment provides constraints such that well-defined conformational itineraries are observed. These conformational itineraries may differ from those observed for chemically-catalyzed reactions in the gas or condensed phase, but nonetheless must still obey stereoelectronic dictates of chemical reactivity. The study of conformational itineraries of enzymes has been assisted by the full spectrum of kinetic, computational and structural methods.[1,2] In the case of glycoside hydrolases, conformational itineraries are often assigned through determination of the three-dimensional structures of ligands bound to enzymes, most commonly substrate (Michaelis), intermediate, and product complexes, and by using inhibitors that mimic the transition state.[3]

GHs have been grouped into >150 families on the basis of primary sequence and ability to cleave specific glycoside substrates.[4,5] As sequence defines the three-dimensional structure of proteins, family members typically adopt similar folds and possess highly conserved amino acids within their active site clefts. The chemical mechanisms through which family members perform catalysis tend to be conserved across a family and lead to substrate hydrolysis with either retention or inversion of anomeric stereochemistry.[6] Inversion of stereochemistry occurs in a single step reaction when water acts as a nucleophile. Retention of stereochemistry is typically achieved through a two-step substitution mechanism involving participation by an enzymic nucleophile or by a pendant neighboring group on the substrate.[6–8] Both pathways benefit from enzymatic amino acids that provide general acid catalysis to promote the departure of the anomeric groups, and general base catalysis to promote nucleophilic attack by water. In almost all cases the transition states possess oxocarbenium-ion-like character and the stability of this TS is greatest when partial double bond character is maximized between C1 and O5, which occurs when the system C5–O5–C1–C2 is planar.[9] Such transition-state conformations include two boats: $B_{2,5}$ and $^{2,5}B$; two half-chairs: $^{4}H_3$ and $^{3}H_4$ (Fig. 1a); and the related envelopes: ^{3}E, E_3, ^{4}E and E_4. As transition state mimicry is a powerful strategy for inhibitor design, efforts have been made to assign conformational itineraries, and in particular the TS conformation, for a large number of GH families.[1,2]

Mannosidases and mannanases catalyze the hydrolysis of mannoside linkages and these enzymes are found within 11 GH families. Enzymes within families GH2, 5, 26, 38, 76, 92, 99, 113, 125 and 134 perform catalysis through itineraries along the $^{O}S_2$–$B_{2,5}$–$^{1}S_5$ region of conformational space whereas enzymes of families GH47 and 134 react through the $^{3}S_1$–$^{3}H_4$–$^{1}C_4$ conformational axis (Fig. 1b). The use of mannoimidazole and analogues thereof have been instrumental in the assignment of conformational itineraries and transition state conformation (Table 1).

In the case of family GH125, the conformational itinerary remained elusive for many years. Initial X-ray structures of the foundation member *Cp*GH125 *exo*-α-1,6-mannosidase (*Cp*GH125) with the nonhydrolyzable substrate mimic methyl 1,6-α-thiomannobioside (**1**) (Protein Databank (PDB) ID: 3QT9) and deoxymannojirimycin (**2**) (PDB ID: 3QRY) revealed undis-

[a]*York Structural Biology Laboratory, Department of Chemistry, The University of York, YO10 5DD York, UK. E-mail: gideon.davies@york.ac.uk*
[b]*School of Chemistry and Bio21 Molecular Science and Biotechnology Institute, University of Melbourne, Melbourne, Victoria 3010, Australia. E-mail: sjwill@unimelb.edu.au*

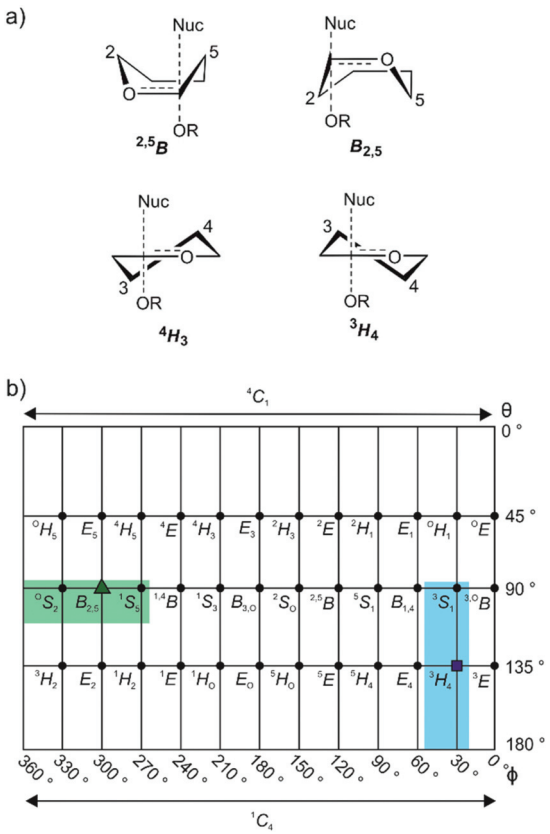

Fig. 1 (a) Common half-chair and boat transition state conformations, illustrated for α-glycosidases. (b) Common mannosidase conformational itineraries shown on a Mercator plot with that for GH125 highlighted in green. Shown in blue is the $^{3}S_{1}$–$^{3}H_{4}$–$^{1}C_{4}$ itinerary used by GH47 and 134 enzymes. The transition states are represented by a green triangle and a blue square.

Table 1 Proposed transition state conformation of mannosidases from various glycoside hydrolase families. Families for which the transition state conformation has been assigned on the basis of mannoimidazole complexes are indicated with an asterisk (*)

	Transition state conformation	
	$^{3}H_{4}{}^{‡}$	$B_{2,5}{}^{‡}$
α-Mannosidases	47* (ref. 10)	38*,[3] 76,[11] 92*,[12] 125*[a]
β-Mannosidases	134 (ref. 13)	2*,[14] 5*,[15] 26*,[3,16] 113*,[3] 130 [17]

[a] This work.

torted, ground-state $^{4}C_{1}$ conformations (Fig. 2a).[18] Instead, a computational approach involving *ab initio* QM/MM metadynamics was used to model the conformation of substrate, 1,6-α-mannobiose, in the enzyme active site, by *in silico* substitution of the sulfur in the experimentally determined X-ray structure.[19] This calculation predicted that the *O*-glycoside favoured an $^{O}S_{2}$ conformation on-enzyme and hinted at an $^{O}S_{2} \rightarrow B_{2,5}{}^{‡} \rightarrow {}^{1}S_{5}$ conformational itinerary, which was fully supported by QM/MM simulations of the reaction mechanism (Fig. 2b). Direct experimental support for this mechanism was obtained through determination of the Michaelis complex for the catalytically-disabled acid mutant (D220N) of *Cp*GH125 in complex with 1,6-α-mannobiose, which revealed an $^{O}S_{2}$ conformation consistent with the computational predictions.[19]

As the ultimate determinant of the activation barrier for catalysis, the TS is the cardinal feature of the conformational itinerary. Mannoimidazole (**3**) (MIm) has emerged as a powerful chemical probe for TS conformation of mannosidases owing to its flattened nature, with an sp^{2}-hybridized anomeric centre and energetically feasible access to all of the possible stereoelectronically-compliant conformations expected for an oxocarbenium ion-like transition state (Fig. 2b).[3] Indeed, for a single step reaction, determination of the conformation of the transition state allows prediction of the conformational itinerary (from substrate to product *via* the TS) by invoking the principle of least nuclear motion.[21] This principle states that elementary reactions that involve the least change in atomic position and electronic configuration will be favoured. Given the importance of the TS conformation in a reaction coordinate, and the utility of MIm in assigning conformational itineraries, we chose to revisit family GH125 to gather additional evidence in support of the proposed conformational itinerary. Here we report an X-ray structure of mannoimidazole (**3**) bound to wild-type *Cp*GH125 that provides compelling evidence in support of a 'latitudinal' $^{O}S_{2} \rightarrow B_{2,5}{}^{‡} \rightarrow {}^{1}S_{5}$ conformational itinerary, complementing previous computational and structural data.

Results and discussion

Glycoimidazoles have been argued to act as glycosidase inhibitors through 'lateral' protonation of the imidazole nitrogen lone pair by the enzymatic general acid approaching in the plane of the imidazole ring.[22] In fact, this interaction served as the basis for an early classification of glycosidases into *syn* and *anti* protonators, based on whether their general acid residues are situated *syn* or *anti* to the substrate C1–O5 bond (Fig. 2c).[23] However, analysis of published complexes with GH125 enzymes shows that the general acid residue is located below the mean plane of the ring,[18,19] suggesting that there are poor prospects for binding of MIm to *Cp*GH125. Yet, there are now several examples of glycoimidazoles binding to glycosidases with good affinity even without achieving a prototypical interaction between the enzymatic general acid and the imidazole nitrogen, such as β-glucosidases of family GH116,[24] α-mannanases of family GH99[25] and α-mannosidases of family GH47[10] (Fig. 2d). The success of these cases inspired us to investigate binding of MIm to *Cp*GH125.

We studied the thermodynamics for binding of MIm to *Cp*GH125 using isothermal titration calorimetry (Fig. 3a). Analysis of the calorimogram using a one site binding model allowed prediction of binding at 3.2 sites with an overall K_{D} value of 1.6 mM. Using a sequential binding site model, individual dissociation constants can be calculated at each site yielding values of 40 μM, 105 μM, and 3.1 mM. However, whilst this is indicative of multiple binding sites, it is not clear that the individual K_{D} values are accurately determined by the

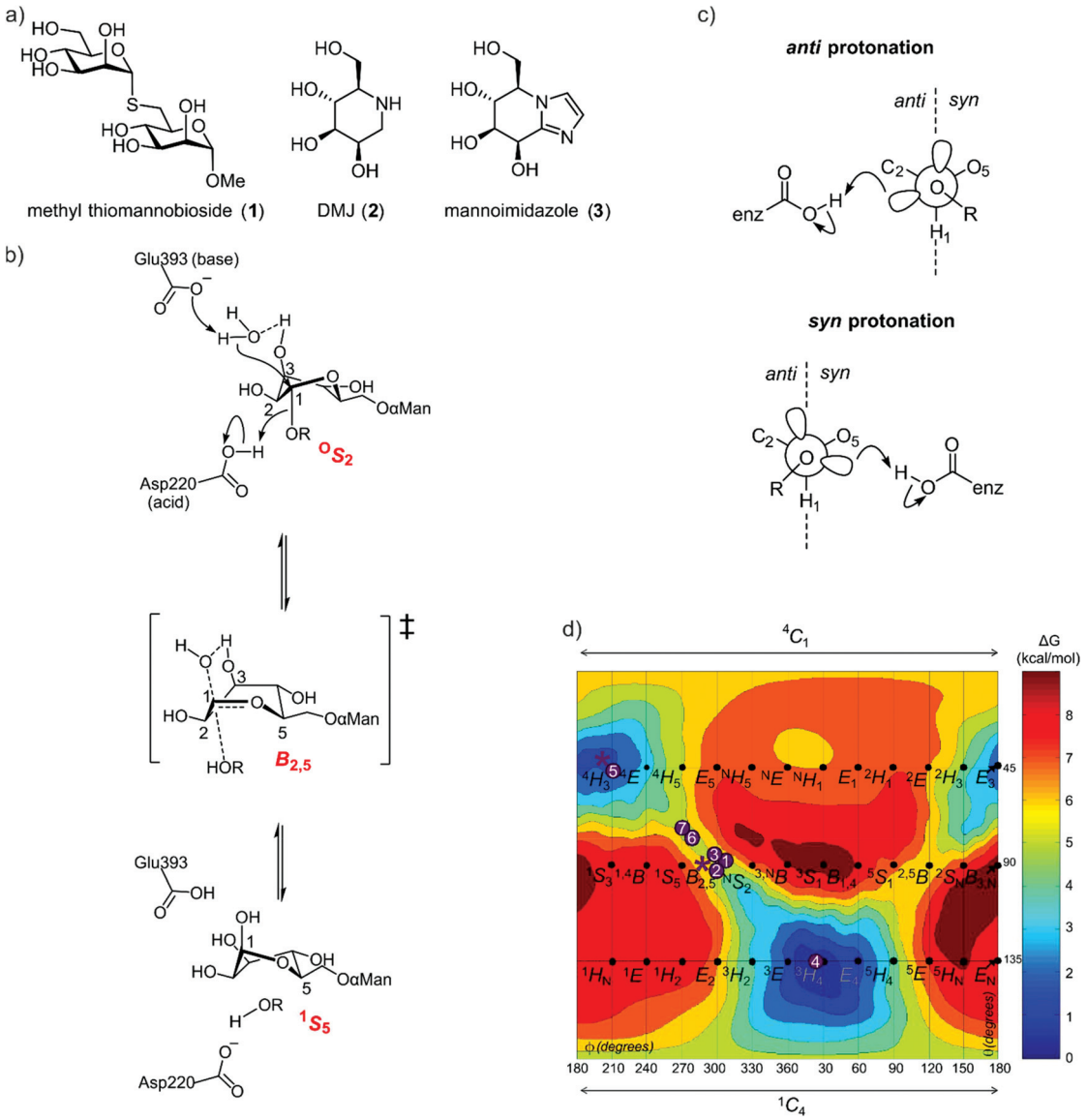

Fig. 2 (a) Structures of methyl α-thiomannobioside, deoxymannojirimycin and mannoimidazole. (b) Mechanism showing distortion of mannose from an $^{O}S_2$ conformation to $^{1}S_5$, *via* a $B_{2,5}$ transition state, a credible conformational itinerary of GH125 α-mannosidases. (c) *syn* and *anti* trajectory of the protonator/general acid residue in respect to the carbohydrate ligand. (d) Conformational free energy landscape of mannoimidazole in complex with a variety of GH family mannosidases. **1** + **2**: β-Man-1,4-MIm bound to GH26 *Cj*Man26C and GH113 *Aa*ManA;[3] **3**: MIm bound to GH2 *Bt*Man2A;[14] **4**: MIm bound to GH47 *Ck*Man47;[10] **5** + **6**: MIm bound to GH38 *Dm*GManII;[3,20] **7**: MIm bound to GH92 *Bt*Man3990;[12] * (asterisk) represent MIm bound to *Cp*GH125 (this work).

data. In order to gain evidence that binding by MIm, as shown by ITC, results in enzyme inhibition, we determined its IC_{50} value. At a concentration of 0.5 mM DNPMan, we determined an IC_{50} of 1.7 mM (Fig. 3b), consistent with the overall ITC figure of 1.6 mM; this IC_{50} value cannot be converted to a K_I value since the substrate does not give saturation kinetics and so K_M cannot be determined.

Binding stoichiometry of >1 for basic sugar-shaped heterocycles is unusual and suggests that the ligand may not solely be binding at the −1 subsite. Previous work has identified three subsites, −1, +1 and +2, in *Cp*GH125 through a complex with 1,6-α-mannotriose (PDB ID: 5M7Y),[19] and studies of a disaccharide substrate that binds in the −1/+1 subsites revealed saturation kinetics, whereas a monosaccharide substrate, 2,4-dinitrophenyl α-mannoside (DNPMan), that bound only in the −1 subsite did not.[18,26] Previous poor electron density in the +2 subsite suggests that this may represent the low affinity binding site, a conclusion supported by subsequent X-ray crystallographic studies (*vide infra*). The two tighter affinities therefore should likely reflect binding at the −1 and +1 subsites; however, we cannot draw conclusions as to which value is assigned to each of these subsites. Nevertheless, the interesting ITC data encouraged efforts to determine the 3D structure of a complex of *Cp*GH125 with mannoimidazole.

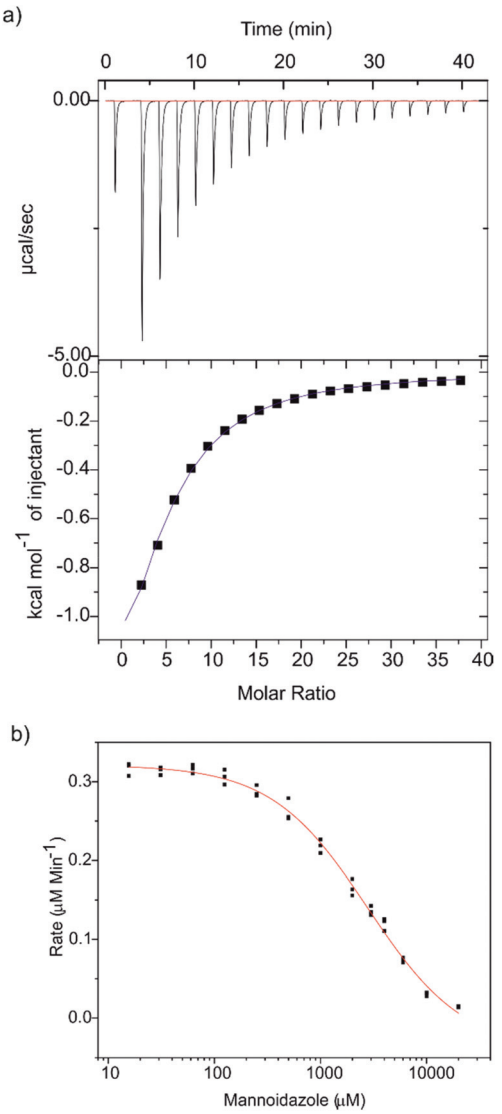

Fig. 3 (a) Raw thermodynamic data obtained by isothermal titration calorimetry. Top: injection profile with the baseline in red; bottom: titration curve with the fitting curve in blue. (b) IC_{50} curve of MIm against GH125 using the monosaccharide substrate DNPMan.

Table 2 Data collection and refinement statistics of CpGH125 and MIm

Resolution [Å]	84.8–1.85 (1.89–1.85)[a]
R_{merge}	0.08 (0.51)
CC(1/2)	0.99 (0.54)
Completeness [%]	99.7 (99.9)
R_{work}/R_{free}	0.20/0.24
$RMSD_{bonds}$ [Å]	0.01
PDB code	6RQK

[a] Values in parentheses are for highest-resolution shell.

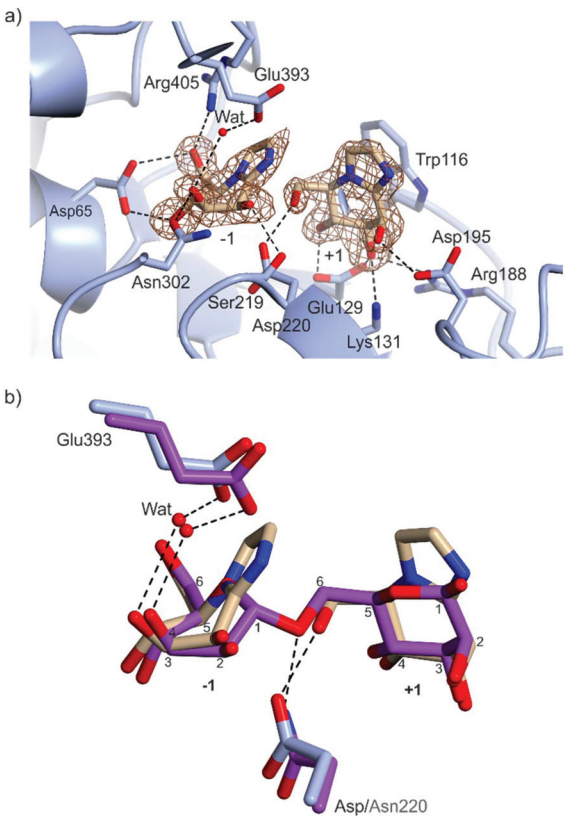

Fig. 4 (a) Complex of *Cp*GH125 with mannoimidazole in the –1 and +1 subsites. The residues of the enzyme that form hydrogen bonding interactions and close contacts with mannoimidazole (<3 Å distance) are shown in blue and the nucleophilic water molecule is depicted by a red sphere. The electron density map is a REFMAC maximum-likelihood/σA-weighted 2 $F_o - F_c$ synthesis contoured at 0.75 electrons $Å^{-3}$ and 1.20 electrons $Å^{-3}$ clipped to MIm in the –1 and +1 subsite, respectively. (b) Superposition of *Cp*GH125 in complex with MIm (monomer A) and 1,6-α-mannobiose (PDB ID: 5M7I), shown in purple. Hydrogen bonds shown in black between the catalytic residues of *Cp*GH125 and nucleophilic water.

Preformed crystals of *Cp*GH125 recombinantly expressed in *E. coli* were soaked with MIm and the structure of the complex was solved at 1.85 Å resolution (Table 2). The crystal form contains 2 monomers in the asymmetric unit. Density for MIm was observed both in the −1 and +1 subsites, but not in the +2 subsite (Fig. 4a). The MIm molecule in the −1 subsite bound in a $B_{2,5}$ conformation and the MIm molecule in the +1 subsite bound in a $^4H_3$ conformation. The occupancy of MIm in the −1 subsite was estimated to be 80% and 70% for monomer A and B, respectively; the occupancy of MIm in the +1 subsite was 100% for both monomers. These observations are consistent with tight binding of MIm at the −1/+1 subsites, and weaker binding at the +2 subsite.

MIm molecules in each site engage with a range of active site residues (Fig. 4a). Key interactions with the −1 subsite MIm include the carbonyl oxygen of Ser219 with O2, Oδ1 of Asn302 with O3, Oδ1 and Oδ2 of Asp65 with O4 and O6, respectively, and NH_2 of Arg405 with O6. The general base Glu393 is 2.3 Å away from a water poised for inline attack at the 'anomeric carbon' of MIm. Major interactions with MIm in subsite +1 include Oδ1 of Asp195 with O2, Glu129 Oε1 with O3 and Oε2 with O4, and the terminal amine nitrogen, NZ of Lys131 and NH_2 of Arg188 with O3. The catalytic amino acid,

Asp220, interacts with O6 of MIm in the +1 subsite. Trp116 is stacked parallel to the imidazole of MIm, with CZ2 of Trp119 and N2 of MIm spaced 3.79 Å apart.

Overlay of the complex of MIm with wildtype *Cp*GH125 with that of the D220N mutant of the same enzyme with 1,6-α-mannobiose (PDB ID: 5M7I) is shown in Fig. 4b. This shows that the two MIm molecules bind such that their carbohydrate rings are well-matched with the equivalent mannose rings of 1,6-α-mannobiose. Moreover, the general acid (Asp220; or variant Asn220), and general base (Glu393) residues occupy similar positions in space. This overlay highlights that the interaction of Asp220 with the +1 subsite MIm molecule, in the complex determined here, can be considered equivalent to the interaction of Asn220 with the inter-glycosidic oxygen of 1,6-α-mannobiose seen in the *Cp*GH125-D220N complex. Both complexes include a well-defined water molecule hydrogen-bonded to Glu393 and O3 of the −1 subsite MIm that is poised to undertake a nucleophilic attack at the anomeric centre. The interaction of this water molecule with O3 assists in orientating the water molecule to perform an in-line attack on C1 (Fig. 2b).

Nerinckx generalized the concept of *syn*/*anti* protonation to consider divergence from canonical orientation in the mean plane of the ring to include orientations in a *syn* or *anti* hemisphere (Fig. 2c).[27] According to this extended concept, *Cp*GH125 can be considered a *syn* protonator and with the present work *Cp*GH125 joins a growing list examples of glycosidases that can bind glycoimidazoles even without achieving lateral protonation. While binding is seen in this and related cases, presumably the potency of binding is less than what might be expected for an ideally located general acid that can achieve such an interaction, an expectation that is borne-out by much tighter binding to canonical anti-protonators such as *Bt*3130 and *Bt*3965 from *Bacteroides thetaiotaomicron* GH92 (K_i = 1.0 and 0.4 μM, respectively) whereas other α-mannosidases from *B. thetaiotaomicron* have a K_i values ranging from 40–6000 μM.[12] Also, imidazole-substituted mannoimidazoles can exhibit even tighter binding, for example, the β-mannosidase *Bt*Man2A (from family GH2) binds phenethyl-mannoimidazole with K_i = 57 nM compared to binding to mannoimidazole with K_i = 1400 nM.[14] In this case since the inhibitor lies across both the −1 and +1 subsite, the number of interactions the inhibitor can make with the protein increases. We highlight one important anomalous case, in which a complex of a disaccharide MIm analogue with *Bx*GH99 1,2-α-mannanase revealed an unusual $^2H_3/E_3$ conformation possibly due to steric clashes with an active site residue, Tyr252.[25] In this case no K_D value could be measured by ITC indicating poor affinity for the enzyme.

Conclusions

The present work builds upon prior computational and structural studies of *Cp*GH125 focussed on the Michaelis complex that provided evidence for an $^{O}S_2 \rightarrow B_{2,5}^{\ddagger} \rightarrow {}^{1}S_5$ conformational itinerary (Fig. 4). The present TS mimicking complex with MIm in a $B_{2,5}$ conformation provides compelling evidence for this conformation in the transition state of this enzyme. Since the free energy landscape[3] for MIm reveals that the most stable conformations for this inhibitor in the gas phase are the $^4H_3$ and $^3H_4$ conformations, with the $B_{2,5}$ conformation some 6 kcal mol^{-1} less stable, the observation of a $B_{2,5}$ conformation provides persuasive evidence that this conformation is induced upon binding because of the enzyme's strong preference for stabilizing a transition state with this conformation. Combined with the previously published Michaelis complex in an $^{O}S_2$ conformation, we now have crystallographic 'snapshots' of states that together define two of the three critical points along the reaction coordinate of family GH125 enzymes.

Experimental

Expression, purification and crystallisation of *Cp*GH125$_{WT}$

Wild-type *Cp*GH125 was expressed and purified under the same conditions as the mutant, *Cp*GH125-D220N.[19] *Cp*GH125, at 12 mg ml^{-1}, was crystallised under 0.2 M $MgCl_2$, 0.1 M HEPES pH 7.0 and 24% PEG 3350, protein : reservoir ratio 0.3 : 0.5 μL conditions and subsequently soaked with mannoimidazole. Crystals were soaked in 5 mM inhibitor for 2 h at 20 °C and then cryoprotected stepwise in 25% ethylene glycol before snap freezing in liquid nitrogen.

Data were collected on Diamond MX beamline I24 and processed using xia2 3dii.[28] Integrated data were processed using the CCP4 software suite;[29] the programs used were aimless,[30,31] MOLREP[32] with 5M7I as the reference model and cycles of REFMAC5[33–38] and COOT[39] for refinement of the structure. *Cp*GH125 structures figures were produced using CCP4 mg.[40] Coordinate and observed structure-factor amplitudes have been deposited on the PDB with accession code 6RQK.

Measurement of dissociation constant (K_D) by isothermal titration calorimetry

*Cp*GH125 and MIm were buffer matched by dialysis into 20 mM HEPES pH 7.0 and 200 mM NaCl. MIm was added by syringe to a solution of *Cp*GH125 in the calorimeter cell using a MicroCal ITC_{200} calorimeter at 25 °C with 20 injections. The concentration of *Cp*GH125 was 200 μM and the ligand concentration was varied between 4 mM and 36 mM to obtain a consistent K_D value. The binding affinity was obtained using one site fitting and a sequential binding fit (3 sites) within the Origin7 software. The association constant (K_A) was converted to a dissociation constant using the equation $K_D = 1/K_A$. An average over 5 experiments was taken to obtain accurate K_D values for the three subsites.

Measurement of inhibition constant (IC_{50}) of MIm

Enzyme assays were performed in 40 μL quartz cuvettes with path lengths of 10 mm. Change in absorbance values at 405 nm were monitored using a Cary UV-Vis spectrophoto-

meter. Reactions were initiated by addition of *Cp*GH125 at 9.05 μM to a solution of 0.5 mM DNPMan in PBS buffer (pH 7.4) at 37 °C. Rates were measured by observing change in absorption for 3 min. Each reaction was performed in triplicate and averaged, and the data fit to a Hill plot.

Conflicts of interest

There are no conflicts to declare.

Acknowledgements

This research was funded by Biotechnology and Biological Sciences Research Council (grant BB/M011151/1) for support AM. SJW is funded by the Australian Research Council (DP180101957, DP160100597). GJD is the Royal Society Ken Murray Research Professor. We thank Diamond Light Source for access to beamline I24 (proposal number mx-9948-71) that contributed to the results presented here and Johan Turkenburg and Sam Hart for coordinating data collection. PDB accession code: 6RQK. We would also like to thank Zach Armstrong for support with the IC_{50} enzyme assay.

Notes and references

1 G. J. Davies, A. Planas and C. Rovira, *Acc. Chem. Res.*, 2012, **45**, 308–316.
2 G. Speciale, A. J. Thompson, G. J. Davies and S. J. Williams, *Curr. Opin. Struct. Biol.*, 2014, **28**, 1–13.
3 R. J. Williams, J. Iglesias-Fernández, J. Stepper, A. Jackson, A. J. Thompson, E. C. Lowe, J. M. White, H. J. Gilbert, C. Rovira, G. J. Davies and S. J. Williams, *Angew. Chem., Int. Ed.*, 2014, **53**, 1087–1091.
4 V. Lombard, H. Golaconda Ramulu, E. Drula, P. M. Coutinho and B. Henrissat, *Nucleic Acids Res.*, 2014, **42**, D490–D495.
5 B. Henrissat and A. Bairoch, *Biochem. J.*, 1996, **316**(Pt 2), 695–696.
6 D. E. Koshland, *Biol. Rev.*, 1953, **28**, 416–436.
7 M. L. Sinnott, *Chem. Rev.*, 1990, **90**, 1171–1202.
8 J. D. McCarter and G. Stephen Withers, *Curr. Opin. Struct. Biol.*, 1994, **4**, 885–892.
9 R. J. Woods, C. W. Andrews and J. P. Bowen, *J. Am. Chem. Soc.*, 1992, **114**, 859–864.
10 A. J. Thompson, J. Dabin, J. Iglesias-Fernández, A. Ardèvol, Z. Dinev, S. J. Williams, O. Bande, A. Siriwardena, C. Moreland, T.-C. Hu, D. K. Smith, H. J. Gilbert, C. Rovira and G. J. Davies, *Angew. Chem., Int. Ed.*, 2012, **51**, 10997–11001.
11 A. J. Thompson, G. Speciale, J. Iglesias-Fernández, Z. Hakki, T. Belz, A. Cartmell, R. J. Spears, E. Chandler, M. J. Temple, J. Stepper, H. J. Gilbert, C. Rovira, S. J. Williams and G. J. Davies, *Angew. Chem., Int. Ed.*, 2015, **54**, 5378–5382.
12 Y. Zhu, M. D. L. Suits, A. J. Thompson, S. Chavan, Z. Dinev, C. Dumon, N. Smith, K. W. Moremen, Y. Xiang, A. Siriwardena, S. J. Williams, H. J. Gilbert and G. J. Davies, *Nat. Chem. Biol.*, 2010, **6**, 125–132.
13 Y. Jin, M. Petricevic, A. John, L. Raich, H. Jenkins, L. Portela De Souza, F. Cuskin, H. J. Gilbert, C. Rovira, E. D. Goddard-Borger, S. J. Williams and G. J. Davies, *ACS Cent. Sci.*, 2016, **2**, 896–903.
14 L. E. Tailford, W. A. Offen, N. L. Smith, C. Dumon, C. Morland, J. Gratien, M.-P. Heck, R. V. Stick, Y. Blériot, A. Vasella, H. J. Gilbert and G. J. Davies, *Nat. Chem. Biol.*, 2008, **4**, 306–312.
15 F. Vincent, T. M. Gloster, J. Macdonald, C. Morland, R. V. Stick, F. M. V. Dias, J. A. M. Prates, C. M. G. A. Fontes, H. J. Gilbert and G. J. Davies, *ChemBioChem*, 2004, **5**, 1596–1599.
16 A. Tankrathok, J. Iglesias-Fernandez, R. J. Williams, S. Pengthaisong, S. Baiya, Z. Hakki, R. C. Robinson, M. Hrmova, C. Rovira, S. J. Williams and J. R. Ketudat Cairns, *ACS Catal.*, 2015, **5**, 6041–6051.
17 F. Cuskin, A. Baslé, S. Ladevèze, A. M. Day, H. J. Gilbert, G. J. Davies, G. Potocki-Véronèse and E. C. Lowe, *J. Biol. Chem.*, 2015, **290**, 25023–25033.
18 K. J. Gregg, W. F. Zandberg, J.-H. Hehemann, G. E. Whitworth, L. Deng, D. J. Vocadlo and A. B. Boraston, *J. Biol. Chem.*, 2011, **286**, 15586–15596.
19 S. Alonso-Gil, A. Males, P. Z. Fernandes, S. J. Williams, G. J. Davies and C. Rovira, *J. Am. Chem. Soc.*, 2017, **139**, 1085–1088.
20 D. A. Kuntz, C. A. Tarling, S. G. Withers and D. R. Rose, *Biochemistry*, 2008, **47**, 10058–10068.
21 M. L. Sinnott, *Adv. Phys. Org. Chem.*, 1988, **24**, 113–204.
22 A. Varrot, M. Schülein, M. Pipelier, A. Vasella and G. J. Davies, *J. Am. Chem. Soc.*, 1999, **121**, 2621–2622.
23 T. D. Heightman and A. T. Vasella, *Angew. Chem., Int. Ed.*, 1999, **38**, 750–770.
24 R. Charoenwattanasatien, S. Pengthaisong, I. Breen, R. Mutoh, S. Sansenya, Y. Hua, A. Tankrathok, L. Wu, C. Songsiriritthigul, H. Tanaka, S. J. Williams, G. J. Davies, G. Kurisu and J. R. K. Cairns, *ACS Chem. Biol.*, 2016, **11**, 1891–1900.
25 P. Z. Fernandes, M. Petricevic, L. Sobala, G. J. Davies and S. J. Williams, *Chem. – Eur. J.*, 2018, **24**, 7464–7473.
26 L. Deng, P. Tsybina, K. J. Gregg, R. Mosi, W. F. Zandberg, A. B. Boraston and D. J. Vocadlo, *Bioorg. Med. Chem.*, 2013, **21**, 4839–4845.
27 W. Nerinckx, T. Desmet, K. Piens and M. Claeyssens, *FEBS Lett.*, 2005, **579**, 302–312.
28 G. Winter, *J. Appl. Crystallogr.*, 2010, **43**, 186–190.
29 M. D. Winn, C. C. Ballard, K. D. Cowtan, E. J. Dodson, P. Emsley, P. R. Evans, R. M. Keegan, E. B. Krissinel, A. G. W. Leslie, A. McCoy, S. J. McNicholas, G. N. Murshudov, N. S. Pannu, E. A. Potterton, H. R. Powell, R. J. Read, A. Vagin and K. S. Wilson, *Acta Crystallogr., Sect. D: Biol. Crystallogr.*, 2011, **67**, 235–242.
30 P. Evans, *Acta Crystallogr., Sect. D: Biol. Crystallogr.*, 2006, **62**, 72–82.

31 P. R. Evans and G. N. Murshudov, *Acta Crystallogr., Sect. D: Biol. Crystallogr.*, 2013, **69**, 1204–1214.
32 A. Vagin and A. Teplyakov, *Acta Crystallogr., Sect. D: Biol. Crystallogr.*, 2010, **66**, 22–25.
33 G. N. Murshudov, P. Skubák, A. A. Lebedev, N. S. Pannu, R. A. Steiner, R. A. Nicholls, M. D. Winn, F. Long and A. A. Vagin, *Acta Crystallogr., Sect. D: Biol. Crystallogr.*, 2011, **67**, 355–367.
34 G. N. Murshudov, A. A. Vagin and E. J. Dodson, *Acta Crystallogr., Sect. D: Biol. Crystallogr.*, 1997, **53**, 240–255.
35 N. S. Pannu, G. N. Murshudov, E. J. Dodson and R. J. Read, *Acta Crystallogr., Sect. D: Biol. Crystallogr.*, 1998, **54**, 1285–1294.
36 M. D. Winn, G. N. Murshudov and M. Z. Papiz, *Methods Enzymol.*, 2003, **374**, 300–321.
37 A. A. Vagin, R. A. Steiner, A. A. Lebedev, L. Potterton, S. McNicholas, F. Long and G. N. Murshudov, *Acta Crystallogr., Sect. D: Biol. Crystallogr.*, 2004, **60**, 2184–2195.
38 R. A. Nicholls, F. Long and G. N. Murshudov, *Acta Crystallogr., Sect. D: Biol. Crystallogr.*, 2012, **68**, 404–417.
39 P. Emsley, B. Lohkamp, W. G. Scott and K. Cowtan, *Acta Crystallogr., Sect. D: Biol. Crystallogr.*, 2010, **66**, 486–501.
40 S. McNicholas, E. Potterton, K. S. Wilson and M. E. M. Noble, *Acta Crystallogr., Sect. D: Biol. Crystallogr.*, 2011, **67**, 386–394.